Supporting Information: Osmotic Transport at the Aqueous Graphene and hBN Interfaces: Scaling Laws from a Unified, First Principles Description

Laurent Joly,[†,‡] Robert H. Meißner,[¶,§] Marcella Iannuzzi,[‖] and Gabriele Tocci[*,‖]

†*Univ Lyon, Univ Claude Bernard Lyon 1, CNRS, Institut Lumière Matière, F-69622, VILLEURBANNE, France*

‡*Institut Universitaire de France (IUF), 1 rue Descartes, 75005 Paris, France*

¶*Hamburg University of Technology, Insitute of Polymers and Composites, Hamburg, 21073, Hamburg*

§*Helmholtz-Zentrum Hereon, Institute of Surface Science, Geesthacht, 21502, Germany*

‖*Department of Chemistry, Universität Zürich, 8057 Zürich, Switzerland*

E-mail: gabriele.tocci@chem.uzh.ch

Contents

1 Computational details of AIMD simulations

The results in the main manuscript have been obtained with the CP2K/QUICKSTEP package (v.8.1).[S1,S2] CP2K/QUICKSTEP employs mixed Gaussian and plane-wave basis sets and norm-conserving GTH pseudopotentials.[S3,S4] We used short range molecularly optimized double-ζ valence polarized (DZVP-MOLOPT-SR) Gaussian basis functions, which exhibit a

small basis set superposition error.[S5] A 460 Ry cut-off was used for the plane wave expansion. The systems consist of a single ion dissolved in a water film containing 400 molecules and approximately 2 nm-thick, placed above a $2.56 \times 2.46\,\mathrm{nm}^2$ graphene and a $2.61 \times 2.51\,\mathrm{nm}^2$ hBN sheet. The graphene and hBN lattice constants are 2.46 and 2.50 Å, respectively.[S6,S7] Charge neutrality is maintained through a background charge, which compensates for a net positive (negative) charge of the dissolved I^- (K^+) ion. The free energy profiles of the K^+ and I^- ions were calculated from umbrella sampling simulations.[S8] A total of 23 windows were used for each system and the initial atomic configurations of the *ab initio* simulations were obtained from pre-equilibrated umbrella sampling simulations resulting from 1 ns-long FFMD trajectories. Separate umbrella sampling simulations were performed for potassium and iodide adsorption by restraining each ion at different heights $z_{i,0}$ above the sheets with a harmonic bias potential $U_{b,i}(z,t) = k_b/2(z_i(t) - z_{0,i})^2$, where the index i indicates the i-th window, $z_i(t)$ is the instantaneous height of the ion above the sheets, and $k_b = 836.8\,\mathrm{kJ/mol/nm}^2$ is the spring constant. For each umbrella simulation window, the reference height z_0 was moved 0.05 nm further away from the sheet, starting from a height of 0.25 nm. The dynamics were propagated in the NVT ensemble at 300 K within the Born-Oppenheimer approximation, where temperature control was achieved with the Nosé-Hoover chain thermostat with a time constant of 100 fs.[S9] For each umbrella sampling window, the dynamics were propagated for about 40 ps for all systems, except for I^- adsorption on graphene, for which additional 30 ps trajectories were acquired to test for a possible dependence of our results on the length of the simulations (see Section 2). The free energy was reconstructed using umbrella integration.[S10] The first 10 picoseconds were used for equilibration and not included in the analysis, such that the free energy profile of I^- on graphene shown in the main text is extracted from 60 ps-long trajectories and all other free energy profiles result from 30 ps-long trajectories. Additionally, in order to improve the statistical accuracy of the free energy profile in the bulk region (where the ion is at a height above 1 nm), the sampling in the bulk-like umbrella-windows is augmented joining the data obtained from the simulations for one ion on both

sheets (graphene and hBN). In other words, the sampling within the windows where the reference height of I^- (K^+) on graphene is $z_0 > 1$ nm, were used to extract also the free energy of I^- (K^+) adsorption on hBN, and vice versa.

2 Computational details of FFMD simulations

The starting configurations of the *ab initio* umbrella sampling simulations resulted from FFMD umbrella sampling simulations. Dynamics for each window was propagated for 1 ns and the computational set-up was the same as that discussed in the previous section. As reported in our previous work,[S11] we used the force field parameters in Tables S1 and S2, in order to describe the aqueous graphene and aqueous hBN interfaces. Water was modelled with the rigid SPC/E model.[S12] The graphene and hBN were also held rigid during the simulations. To compute cross interactions through the Lorentz-Berthelot mixing rules, graphene was modelled with the DREIDING[S13] force field and hBN with the *ab initio* derived force-field of Ref. S14. The water/graphene interactions were described with a Lennard-Jones potential according to Ref. S15 and the Lennard-Jones interaction parameters between water and the hBN sheet were obtained from Ref. S14. The Lennard-Jones interaction parameters of I^- at the aqueous graphene interface were described following Ref. S16, whereas the parameters of K^+ adsorption at the aqueous graphene interface, and of both I^- and of K^+ at the aqueous hBN interface were obtained from Ref. S17, where Lorentz-Berthelot mixing rules were used for the B-I^- and N-I^- interactions, as well as for the B-K^+ and N-K^+ and C-K^+ interactions. Finally, the partial charges of the ions were described following Ref. S17, except for I^-, which partial charge was described according to Ref. S16.

Table S1: Lennard-Jones parameters for the different atom pairs used in the FFMD simulations for equilibration.

atoms	σ (Å)	ϵ (kJ/mol)
C–O	3.190	0.392
B–O	3.236	0.434
N–O	3.191	0.359
O–O	3.166	0.650
I^-–O	4.145	0.521
I^-–C	4.169	0.708
I^-–N	3.643	0.611
I^-–B	4.815	0.295
K^+–O	3.001	1.081
K^+–C	3.346	0.327
K^+–N	3.090	1.937
K^+–B	3.635	0.934

Table S2: Partial charges for different atoms used in the FFMD simulations for equilibration.

atom	partial charge (e)
C	0.0000
B	+0.9070
N	−0.9070
O	−0.8476
H	+0.4238
I^-	−0.8000
K^+	+1.0000

3 Validation of the transport coefficients with respect to the time of the AIMD simulations

We remind the reader that the *ab initio* umbrella sampling simulations of I^- adsorption at the aqueous graphene are about 30 ps longer than the simulations for the other systems – *i.e.* 70 ps as opposed to 40 ps, where however the initial 10 ps are left out of the analysis and only used for equilibration. In this section we test the convergence of our results on the osmotic transport on graphene with respect to the length of the trajectories of the *ab initio* umbrella sampling simulations. Specifically, Fig. S1 shows a comparison between the osmotic transport coefficients on graphene obtained over the full length of the umbrella sampling simulations and those obtained computing the free energy of I^- adsorption only from the first part of the trajectory, *i.e.* from 10 to 40 ps, the same as that of K^+ adsorption. It can be seen that although the osmotic transport coefficients display quantitative differences, the scaling behaviour is not altered by the duration of the I^- adsorption simulations.

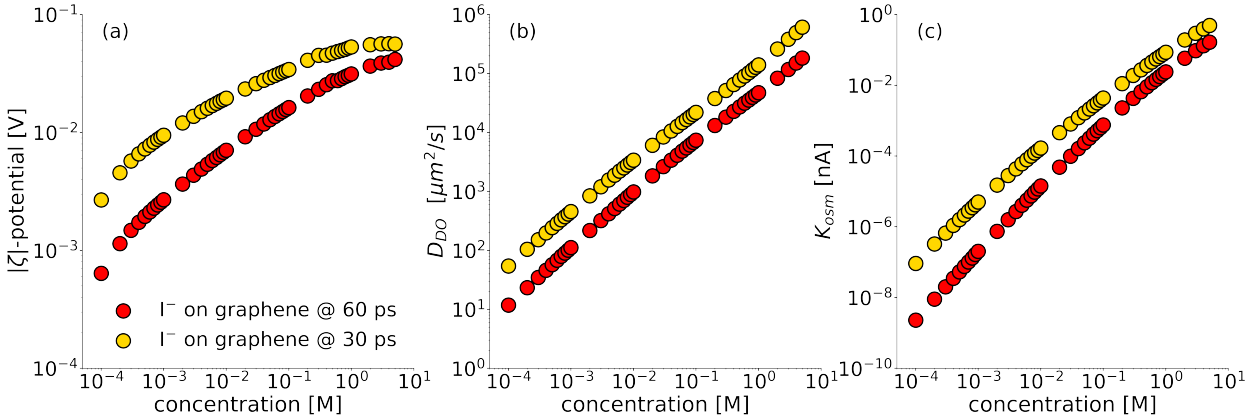

Figure S1: Dependence of the osmotic transport coefficients on the length of the *ab initio* umbrella sampling simulations of I^- adsorption on graphene. The red symbols refer to the osmotic transport coefficients on graphene obtained over the full length of the umbrella sampling simulations, where the free energy of I^- and K^+ adsorption results from about 60 ps-long and 30 ps-long trajectories, respectively. The symbols in yellow instead show the transport coefficients obtained computing the free energy of I^- adsorption only from the first part of the trajectory, *i.e.* from 10 ps to 40 ps, as for the adsorption of K^+.

4 Dipole orientation of water at the aqueous graphene and hBN interfaces

We suggest that subtle differences in the water dipole orientation on graphene and hBN are responsible for the distinct features of the free energy profile of I^- on the two sheets reported in Fig. 2 in the main text. Fig. S2(a) displays the average dipole orientation of water as a function of the distance from the sheets, which is expressed as $\cos\Psi$, where Ψ is the angle between the water bisector and the surface normal and is weighted by the water density ρ_{H_2O}. Whereas the water density profile is very similar on graphene and hBN (see Fig.2 (c) in the main text), the dipole orientation, especially around first water layer (see shaded area in Fig. S2(a)), exhibits some differences on the two sheets. Although in this layer the water dipoles point away from both sheets, the effect is more pronounced on graphene, indicating a stronger dipole-ion interactions than on hBN.[S18] Fig. S2(b) illustrates that the probability distribution of $\cos\Psi$ computed in the first water layer on graphene is shifted to larger values of $\cos\Psi$, confirming that the water dipoles on graphene are on average more aligned and point further away compared to hBN.

5 Derivation of the expressions for the transport coefficients

5.1 Electro-osmotic mobility

We start by considering the electro-osmotic flow of a 1:1 aqueous electrolyte induced at a planar wall by an electric field along the wall, in the absence of an applied pressure gradient, for which we will detail a derivation presented in *e.g.* Refs. S19,S20. The wall is located at $z = 0$, and the liquid in the $z > 0$ region. An electric field E is applied along the x direction parallel to the wall, which induces an electro-osmotic flow along the x direction,

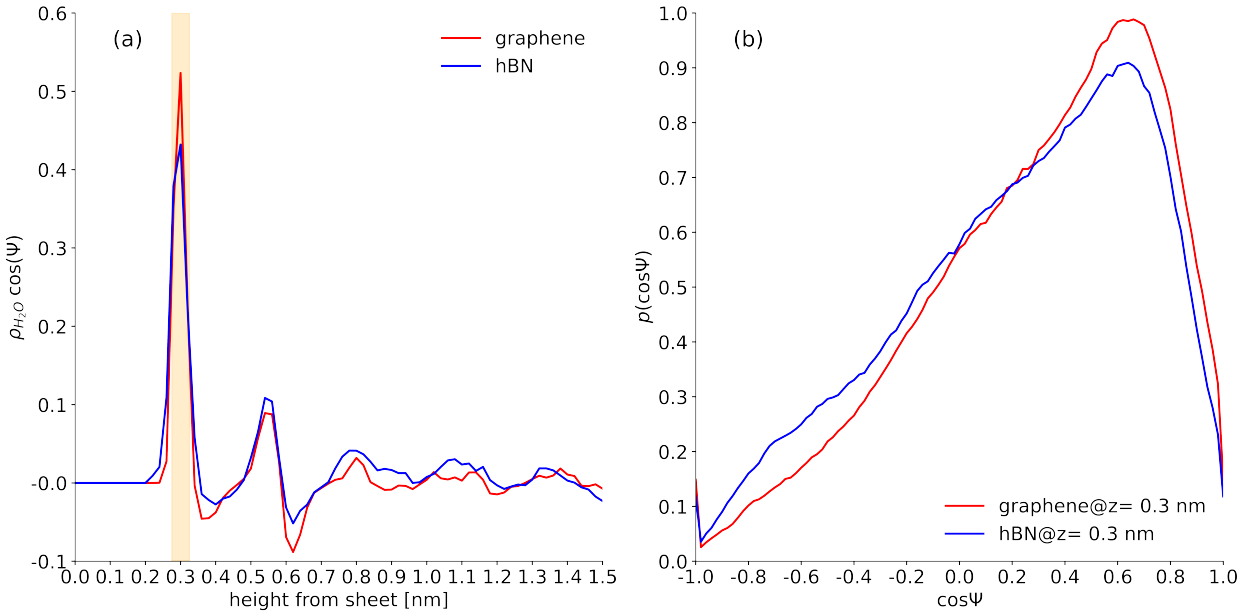

Figure S2: Average dipole orientation of water with respect to the surface normal weighted by the water density profile ($\rho_{\mathrm{H_2O}} \cos\Psi$) as a function of the distance from the sheets (a); and probability distribution of $\cos\Psi$, where water is at a height of 0.3 nm from the surface (b). Values of $\cos\Psi = 1$ and $\cos\Psi = -1$ correspond to water dipoles aligned to the and pointing away and towards the surface, respectively. The shaded bar in (a) is at the height of the first peak in $\rho_{\mathrm{H_2O}} \cos\Psi$ and corresponds to the region where the probability distribution $p(\cos\Psi)$ is calculated in (b).

with a velocity profile $v(z)$. We denote $n_+(z)$, $n_-(z)$ and $\rho_{\mathrm{e}}(z) = q_e\,[n_+(z) - n_-(z)]$ the cation, anion, and charge density profiles, respectively, where q_e is the elementary charge.

The electric field generates a force density $f(z) = \rho_{\mathrm{e}}(z)E$ in the liquid. To compute the induced velocity profile, we assume that the liquid is incompressible, newtonian, and with a homogeneous viscosity η. On hydrophobic, slipping surfaces such as the ones considered in this work, these assumptions have been shown to provide an accurate description of the velocity profiles even in the first molecular layers of the liquid.[S21] In the low Reynolds number limit, one can then write Stokes equation:

$$-\eta \frac{\mathrm{d}^2 v}{\mathrm{d}z^2} = f(z) = \rho_{\mathrm{e}}(z)E. \tag{1}$$

To integrate this equation, we assume that the velocity gradient vanishes far from the wall,

$\mathrm{d}v/\mathrm{d}z|_{z=\infty} = 0$, and we write a partial slip boundary condition[S22] at the wall:

$$v(0) = b \left.\frac{\mathrm{d}v}{\mathrm{d}z}\right|_{z=0}, \tag{2}$$

with b the slip length.[S22] One can then calculate the electro-osmotic velocity far from the wall:

$$v_{\mathrm{eo}} = v(\infty) = \frac{1}{\eta}\int_0^\infty \mathrm{d}z\,(z+b)\rho_{\mathrm{e}}(z)E. \tag{3}$$

Finally, recalling that the electro-osmotic response is commonly quantified by the so-called zeta potential ζ, which relates the electro-osmotic velocity v_{eo} to the electric field E through the Helmholtz-Smoluchowski relation, $v_{\mathrm{eo}} = -(\varepsilon\zeta/\eta)E$ (with ε the bulk liquid permittivity), we obtain the final expression for the zeta potential, reproduced in the main text:

$$\zeta = -\frac{\eta v_{\mathrm{eo}}}{\varepsilon E} = -\frac{1}{\varepsilon}\int_0^\infty \mathrm{d}z\,(z+b)\rho_{\mathrm{e}}(z). \tag{4}$$

Note that no assumption was made on the dielectric permittivity of the system: the bulk dielectric permittivity ε only appears in Eq. (4) through the Helmholtz-Smoluchowski definition of ζ.

5.2 Diffusio-osmotic mobility

5.2.1 Diffusio-osmotic flow

Following a very similar approach, we now consider the diffusio-osmotic flow of a 1:1 aqueous electrolyte induced at a planar wall by a gradient of salt concentration along the wall, in the absence of pressure gradient. Again, the wall is located at $z = 0$, and the liquid in the $z > 0$ region. A gradient of the salt concentration n_{s} far from the wall is applied along the x direction parallel to the wall, which induces a diffusio-osmotic flow along the x direction, with a velocity profile $v(z)$. In the following, all quantities depend implicitly on x and we denote $\nabla = \partial_x$. We denote $n_+(z)$, $n_-(z)$, and $n_{\mathrm{w}}(z)$ the cation, anion, and water density

profiles, respectively, and $n_\mathrm{s} = n_+^\mathrm{b} = n_-^\mathrm{b}$ and n_w^b their bulk values (*i.e.*, at $z = \infty$).

We will use local thermodynamics to compute the force density driving the flow in the interfacial layer, following Ref. S23. In the water+salt mixture, the Gibbs-Duhem relation can be written $\mathrm{d}p = n_+(z)\mathrm{d}\mu_+ + n_-(z)\mathrm{d}\mu_- + n_\mathrm{w}(z)\mathrm{d}\mu_\mathrm{w}$, where p is the pressure and μ_+, μ_- and μ_w the chemical potential of cations, anions, and water, respectively.

A concentration gradient of component $i = \mathrm{w}, +, -$ along x will lead to a chemical potential gradient $\nabla\mu_i$. The chemical potential for component i is given by:

$$\mu_i = \mu_i^0 + k_\mathrm{B}T \ln n_i^\mathrm{b} + \mu_i^\mathrm{exc}, \tag{5}$$

where μ_i^0 denotes a (constant) reference value, μ_i^exc denotes the excess chemical potential due to intermolecular interactions, and where $n_\pm^\mathrm{b} = n_\mathrm{s}$. Because the bulk solutions are ideal, μ_i^exc does not depend on the salt concentration. Therefore the chemical potential gradients are constant along the z direction, and identical for both ion types:

$$\nabla\mu_\mathrm{s} = \nabla\mu_\pm = \frac{\partial\mu_\pm}{\partial n_\mathrm{s}} \times \nabla n_\mathrm{s} = k_\mathrm{B}T\frac{\nabla n_\mathrm{s}}{n_\mathrm{s}} \tag{6}$$

As the pressure is constant in the bulk, the Gibbs–Duhem relation reduces to $0 = 2n_\mathrm{s}\nabla\mu_\mathrm{s} + n_\mathrm{w}^\mathrm{b}\nabla\mu_\mathrm{w}$, so that $\nabla\mu_\mathrm{w} = -2n_\mathrm{s}\nabla\mu_\mathrm{s}/n_\mathrm{w}^\mathrm{b}$. At a distance z from the surface, a pressure gradient remains, giving a force density:

$$f(z) = -\nabla p(z) = \left[n_+(z) + n_-(z)\right](-\nabla\mu_\mathrm{s}) + n_\mathrm{w}(z)(-\nabla\mu_\mathrm{w}) \tag{7}$$

$$f(z) = \left\{n_+(z) + n_-(z) - 2n_\mathrm{s}\frac{n_\mathrm{w}(z)}{n_\mathrm{w}^\mathrm{b}}\right\}(-\nabla\mu_\mathrm{s}) \tag{8}$$

$$f(z) = \left\{n_+(z) + n_-(z) - 2n_\mathrm{s}\frac{n_\mathrm{w}(z)}{n_\mathrm{w}^\mathrm{b}}\right\}\left(-k_\mathrm{B}T\frac{\nabla n_\mathrm{s}}{n_\mathrm{s}}\right). \tag{9}$$

One can then use the same approach as for electro-osmosis, introducing in Stokes equation

the force density given by Eq. (9), to obtain the diffusio-osmotic velocity far from the wall:

$$v_{\mathrm{do}} = \frac{1}{\eta}\int_0^\infty \mathrm{d}z\,(z+b)\left\{n_+(z)+n_-(z)-2n_{\mathrm{s}}\frac{n_{\mathrm{w}}(z)}{n_{\mathrm{w}}^{\mathrm{b}}}\right\}\left(-k_{\mathrm{B}}T\frac{\nabla n_{\mathrm{s}}}{n_{\mathrm{s}}}\right). \tag{10}$$

Finally, recalling that the diffusio-osmotic response is commonly quantified by the so-called diffusio-osmotic mobility D_{DO}, which relates the diffusio-osmotic velocity in the bulk liquid v_{do} to the gradient of salt concentration n_{s}: $v_{\mathrm{do}} = D_{\mathrm{DO}}(-\nabla n_{\mathrm{s}}/n_{\mathrm{s}})$, we obtain the final expression for the diffusio-osmotic mobility, reproduced in the main text:

$$D_{\mathrm{DO}} = -\frac{v_{\mathrm{do}}}{-\nabla n_{\mathrm{s}}/n_{\mathrm{s}}} = \frac{k_{\mathrm{B}}T}{\eta}\int_0^\infty \mathrm{d}z\,(z+b)\left\{n_+(z)+n_-(z)-2n_{\mathrm{s}}\frac{n_{\mathrm{w}}(z)}{n_{\mathrm{w}}^{\mathrm{b}}}\right\}. \tag{11}$$

5.2.2 Streaming excess solute flux

The diffusio-osmotic mobility can also be computed *via* Onsager reciprocal relations.[S24,S25] Indeed, the diffusio-osmotic response of a channel is described by the following linear response matrix:

$$\begin{pmatrix} q \\ \delta j_s \end{pmatrix} = \begin{pmatrix} \cdot & M_{12} \\ M_{21} & \cdot \end{pmatrix}\begin{pmatrix} -\nabla p \\ -\nabla \mu_{\mathrm{s}} \end{pmatrix}, \tag{12}$$

where $-\nabla p$ and $-\nabla\mu_{\mathrm{s}} = -k_{\mathrm{B}}T\,\nabla n_{\mathrm{s}}/n_{\mathrm{s}}$ are the pressure and chemical potential gradients along the channel, q is the flow rate density (*i.e.* the average flow velocity), and δj_s is the excess solute flux density, which will be defined properly in the following; according to Onsager reciprocal relations,[S24,S25] $M_{12} = M_{21} = M_{\mathrm{DO}}$. From the diffusio-osmotic flow response, one can see that D_{DO} simply relates to the response coefficient: $D_{\mathrm{DO}} = k_{\mathrm{B}}TM_{\mathrm{DO}}$.

We will now derive an expression for M_{DO} considering the reciprocal effect, *i.e.* the streaming excess solute flux generated in a channel by a pressure gradient, in the absence of chemical potential gradient: $\delta j_s = M_{\mathrm{DO}}(-\nabla p)$. To that aim we consider an aqueous electrolyte in a slit channel made of two parallel walls located at $z = 0$ and $z = H$. We denote $n_+(z)$, $n_-(z)$, and $n_{\mathrm{w}}(z)$ the cation, anion, and water density profiles, respectively,

and $n_\mathrm{s} = n_+^\mathrm{b} = n_-^\mathrm{b}$ and n_w^b their bulk values (*i.e.*, at $z = H/2$). A pressure gradient $f_\mathrm{p} = -\nabla p$ is applied along the x direction parallel to the walls, which induces a Poiseuille flow along the x direction with a velocity profile $v(z)$. The Poiseuille flow is described by Stokes equation: $-\eta \frac{\mathrm{d}^2 v}{\mathrm{d}z^2} = f_\mathrm{p}$. The channel is symmetric with regard to $z = H/2$, so that $\frac{\mathrm{d}v}{\mathrm{d}z}\big|_{z=H/2} = 0$, and we consider a partial slip BC on the bottom wall: $v(0) = b \ \frac{\mathrm{d}v}{\mathrm{d}z}\big|_{z=0}$. The resulting flow profile writes:

$$v(z) = \frac{f_\mathrm{p}}{2\eta} \left\{ H(z+b) - z^2 \right\}. \tag{13}$$

The excess solute flux through the channel is defined as the difference between the measured solute flux and the solute flux that would be advected by the Poiseuille flow if the solute density was equal to its bulk value everywhere in the channel, $n_+^\mathrm{b} + n_-^\mathrm{b} = 2n_\mathrm{s}$:

$$\delta J_\mathrm{s} = J_\mathrm{s} - 2n_\mathrm{s} Q = 2w \int_0^{H/2} \left[n_+(z) + n_-(z) \right] v(z) \, \mathrm{d}z - 2n_\mathrm{s} Q, \tag{14}$$

where w is the channel width along the y direction, and Q is the solvent flow rate, defined as the change of solvent volume in the reservoir per unit time. Because in the reservoir the solvent density is equal to its bulk value, Q can be related to the flux of solvent particles (water molecules) *via* $Q = J_\mathrm{w}/n_\mathrm{w}^\mathrm{b}$, *i.e.*, the change in solvent volume per unit time in the reservoir is given by the change in the number of solvent particles per unit time, divided by the bulk solvent density. In fine Q writes:

$$Q = \frac{J_\mathrm{w}}{n_\mathrm{w}^\mathrm{b}} = \frac{2w}{n_\mathrm{w}^\mathrm{b}} \int_0^{H/2} n_\mathrm{w}(z) v(z) \, \mathrm{d}z. \tag{15}$$

Combining Eqs. (14) and (15), one gets:

$$\delta J_\mathrm{s} = 2w \int_0^{H/2} \left\{ n_+(z) + n_-(z) - 2n_\mathrm{s} \frac{n_\mathrm{w}(z)}{n_\mathrm{w}^\mathrm{b}} \right\} v(z) \, \mathrm{d}z. \tag{16}$$

If the densities of ions and water only differ from their bulk values in a thin region close to the wall where $z \ll H/2$, then the integrand in Eq. (16) will only differ from zero in this

same region. In that case, one can linearize the velocity profile in the integral:

$$v(z) \simeq \frac{f_\mathrm{p} H}{2\eta}\,(z+b)\,, \tag{17}$$

and one can extend the upper boundary of the integral to infinity:

$$\delta J_\mathrm{s} = \frac{wHf_\mathrm{p}}{\eta}\int_0^\infty (z+b)\left\{n_+(z)+n_-(z)-2n_\mathrm{s}\frac{n_\mathrm{w}(z)}{n_\mathrm{w}^\mathrm{b}}\right\}\mathrm{d}z. \tag{18}$$

The excess solute flux density is then given by $\delta j_\mathrm{s} = \delta J_\mathrm{s}/(wH)$, and the response coefficient is obtained from $M_\mathrm{DO} = \delta j_\mathrm{s}/f_\mathrm{p}$:

$$M_\mathrm{DO} = \frac{1}{\eta}\int_0^\infty (z+b)\left\{n_+(z)+n_-(z)-2n_\mathrm{s}\frac{n_\mathrm{w}(z)}{n_\mathrm{w}^\mathrm{b}}\right\}\mathrm{d}z. \tag{19}$$

Finally, using $D_\mathrm{DO} = k_\mathrm{B}TM_\mathrm{DO}$, one recovers the expression for D_DO obtained *via* the diffusio-osmotic flow response, Eq. (11).

5.2.3 Electro-osmotic contribution to diffusio-osmosis

Note that here we only described the intrinsic diffusio-osmotic response, *i.e.* the coefficient in Onsager response matrix. However, an additional flow can be generated under a salt concentration gradient, for salt ions with an asymmetric diffusivity, and when the channel boundary conditions impose that there is no electrical current along the flow direction in the bulk liquid.[S26,S27] Indeed, in that case a so-called diffusion electric field E_0 appears to avoid charge separation, which can be computed by writing that the bulk electric current vanishes:

$$j_e = q_e(j_+ - j_-) = 0,\ \text{with } j_\pm = -D_\pm\left(\nabla n_\mathrm{s} \mp \frac{q_e n_\mathrm{s}}{k_\mathrm{B}T}E_0\right) \Rightarrow E_0 = \delta\frac{k_\mathrm{B}T}{q_e}\frac{\nabla n_\mathrm{s}}{n_\mathrm{s}}, \tag{20}$$

with $D_\pm$ the bulk cation and anion self-diffusion coefficients, and $\delta = (D_+ - D_-)/(D_+ + D_-)$. The diffusion electric field creates an electro-osmotic flow, with an osmotic velocity far from

the wall:

$$v_{\mathrm{osm}} = -\frac{\varepsilon\zeta}{\eta} \times E_0 = -\frac{\varepsilon\zeta}{\eta} \times \delta \frac{k_{\mathrm{B}}T}{q_e} \frac{\nabla n_{\mathrm{s}}}{n_{\mathrm{s}}}, \tag{21}$$

so that the effective diffusio-osmotic mobility arising from this mechanism writes:

$$D_{\mathrm{EO}} = \frac{v_{\mathrm{osm}}}{-\nabla n_{\mathrm{s}}/n_{\mathrm{s}}} = \frac{\varepsilon\zeta}{\eta} \times \delta \frac{k_{\mathrm{B}}T}{q_e} = \delta \frac{q_e \zeta}{4\pi \ell_{\mathrm{B}} \eta}, \tag{22}$$

where ζ is obtained from Eq. (4).

Figure S3 compares the intrinsic and electro-osmotic contributions to the diffusio-osmotic response for the aqueous graphene and hBN interface at different salt concentrations, where $\delta = 0.02$ for KI salt.[S27] It can be seen in Fig. S3 that the electro-osmotic contribution to diffusio-osmosis follows the scaling of the ζ-potential. The figure also illustrates that the magnitude of D_{EO} is much smaller than the intrinsic response at all concentrations and for both systems.

5.3 Streaming conductivity

The diffusio-osmotic current response is described by the following linear response matrix:

$$\begin{pmatrix} j_e \\ \delta j_s \end{pmatrix} = \begin{pmatrix} \cdot & M_{12} \\ M_{21} & \cdot \end{pmatrix} \begin{pmatrix} E \\ -\nabla \mu_{\mathrm{s}} \end{pmatrix}, \tag{23}$$

where E and $-\nabla\mu_{\mathrm{s}} = -k_{\mathrm{B}}T\,\nabla n_{\mathrm{s}}/n_{\mathrm{s}}$ are the electric field and the chemical potential gradients along the channel, j_e is the electric current density, and δj_s is the excess solute flux density, defined in the previous section; according to Onsager reciprocal relations,[S24,S25] $M_{12} = M_{21} = M_{\mathrm{de}}$. As discussed in the main text, the diffusio-osmotic current is proportional to the perimeter of the channel cross section P. In order to quantify the intrinsic response of the liquid-solid interface, independently of the channel geometry, we define the so-called diffusio-osmotic conductivity K_{osm}, which relates the diffusio-osmotic current generated per

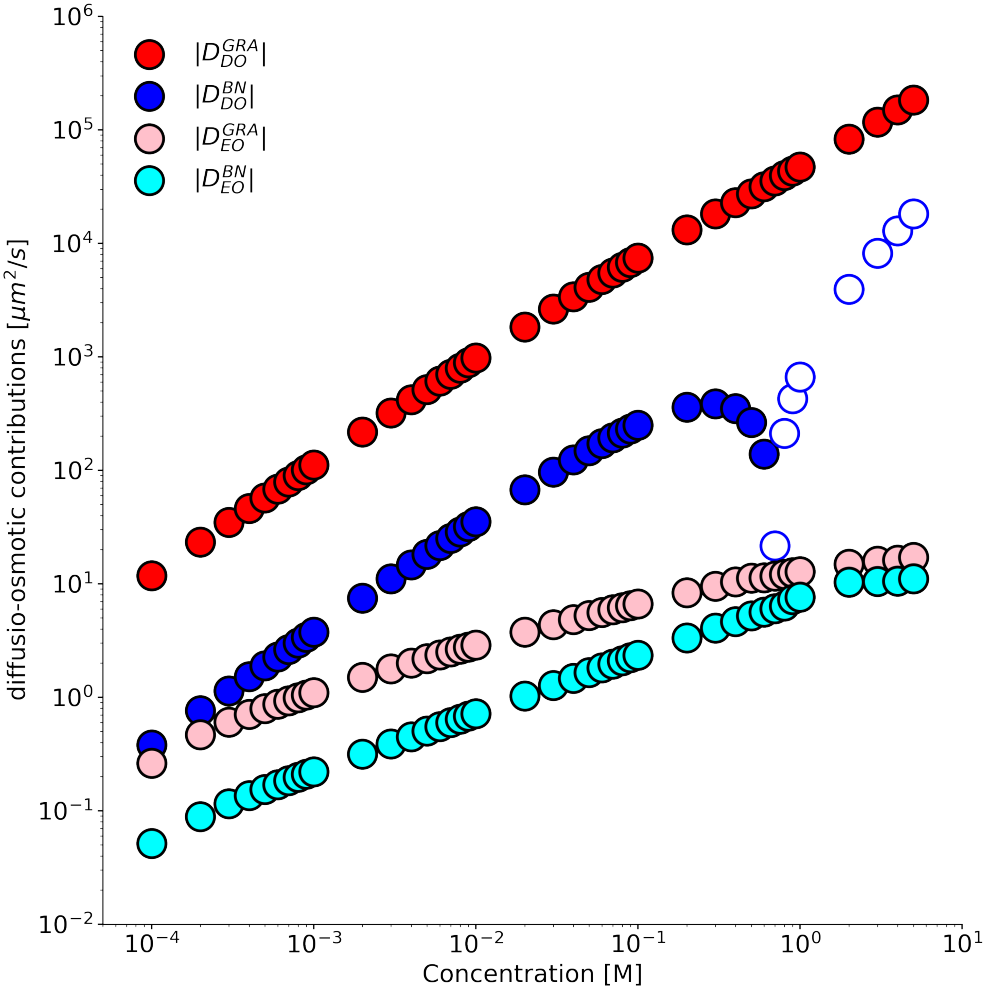

Figure S3: Concentration dependence of the intrinsic and electro-osmotic contributions to the diffusio-osmotic response for the aqueous graphene – respectively $D_{\mathrm{DO}}^{\mathrm{GRA}}$ and $D_{\mathrm{EO}}^{\mathrm{GRA}}$ – and for the aqueous hBN – respectively $D_{\mathrm{DO}}^{\mathrm{BN}}$ and $D_{\mathrm{EO}}^{\mathrm{BN}}$ – interfaces. One can note that $|D_{EO}| \ll |D_{DO}|$ for both graphene and hBN at all considered salt concentrations.

unit length of the channel circumference, I_e/P, to the gradient of salt concentration n_{s}: $I_e/P = K_{\mathrm{osm}}(-\nabla n_{\mathrm{s}}/n_{\mathrm{s}})$; accordingly, denoting S the channel cross section area, K_{osm} simply relates to the response coefficient:

$$K_{\mathrm{osm}} = \frac{S k_{\mathrm{B}} T}{P} M_{\mathrm{de}}. \tag{24}$$

We will now derive an expression for M_{de} by considering the excess solute flux generated in a channel by an electric field, in the absence of chemical potential gradient: $\delta j_s = M_{\mathrm{de}} E$.

As in section 5.2.2, we consider an aqueous electrolyte in a slit channel made of two parallel walls located at $z = 0$ and $z = H$. We denote $n_+(z)$, $n_-(z)$, and $n_\mathrm{w}(z)$ the cation, anion, and water density profiles, respectively, and $n_\mathrm{s} = n_+^\mathrm{b} = n_-^\mathrm{b}$ and n_w^b their bulk values (*i.e.*, at $z = H/2$). An electric field E is applied along the x direction parallel to the walls, which induces an electro-osmotic flow along the x direction with a velocity profile $v(z)$. The electro-osmotic flow is described by Stokes equation: $-\eta \frac{\mathrm{d}^2 v}{\mathrm{d}z^2} = \rho_\mathrm{e}(z) E$, with ρ_e the charge density. The channel is symmetric with regard to $z = H/2$, so that $\frac{\mathrm{d}v}{\mathrm{d}z}\big|_{z=H/2} = 0$, and we consider a partial slip BC on the bottom wall: $v(0) = b \, \frac{\mathrm{d}v}{\mathrm{d}z}\big|_{z=0}$. We also assume a constant dielectric permittivity ε; the validity of this approach is discussed in the next section. The charge density $\rho_\mathrm{e}(z)$ is then related to the electric potential $V(z)$: $\rho_\mathrm{e}(z) = -\varepsilon \frac{\mathrm{d}^2 V}{\mathrm{d}z^2}$. One can then integrate Stokes equation, and the resulting flow profile writes:

$$v(z) = \frac{q_e E}{4\pi \ell_\mathrm{B} \eta} \left[\phi(z) - \phi_\mathrm{s} - 2\,\mathrm{sgn}(\Sigma) \frac{b}{\ell_\mathrm{GC}} \right], \tag{25}$$

with q_e the elementary charge, $\ell_\mathrm{B} = q_e^2/(4\pi\varepsilon k_\mathrm{B} T)$ the Bjerrum length, $\phi = q_e V/(k_\mathrm{B} T)$ the reduced electric potential, ϕ_s its value at the wall, and $\ell_\mathrm{GC} = q_e/(2\pi \ell_\mathrm{B} |\Sigma|)$ the Gouy-Chapman length.[S28]

The excess solute flux through the channel is defined as the difference between the measured solute flux and the solute flux that would be advected by the electro-osmotic flow if the solute density was equal to its bulk value everywhere in the channel, $n_+^\mathrm{b} + n_-^\mathrm{b} = 2n_\mathrm{s}$:

$$\delta J_\mathrm{s} = J_\mathrm{s} - 2n_\mathrm{s} Q = 2w \int_0^{H/2} \left[n_+(z) + n_-(z) \right] v(z)\, \mathrm{d}z - 2n_\mathrm{s} Q, \tag{26}$$

where w is the channel width along the y direction, and Q is the solvent flow rate As discussed in section 5.2.2, Q can be computed as the flux of water molecules divided by the water bulk density:

$$Q = \frac{J_\mathrm{w}}{n_\mathrm{w}^\mathrm{b}} = \frac{2w}{n_\mathrm{w}^\mathrm{b}} \int_0^{H/2} n_\mathrm{w}(z) v(z)\, \mathrm{d}z. \tag{27}$$

Combining Eqs. (26) and (27), one gets:

$$\delta J_{\mathrm{s}} = 2w \int_0^{H/2} \left\{ n_+(z) + n_-(z) - 2n_{\mathrm{s}} \frac{n_{\mathrm{w}}(z)}{n_{\mathrm{w}}^{\mathrm{b}}} \right\} v(z)\, \mathrm{d}z. \tag{28}$$

If the densities of ions and water only differ from their bulk values in a thin region close to the wall where $z \ll H/2$, then the integrand in Eq. (28) will only differ from zero in this same region. In that case, one can extend the upper boundary of the integral to infinity:

$$\delta J_{\mathrm{s}} = \frac{w q_e E}{2\pi \ell_{\mathrm{B}} \eta} \int_0^{\infty} \left\{ n_+(z) + n_-(z) - 2n_{\mathrm{s}} \frac{n_{\mathrm{w}}(z)}{n_{\mathrm{w}}^{\mathrm{b}}} \right\} \left[\phi(z) - \phi_{\mathrm{s}} - 2\,\mathrm{sgn}(\Sigma) \frac{b}{\ell_{\mathrm{GC}}} \right] \mathrm{d}z. \tag{29}$$

The excess solute flux density is then given by $\delta j_{\mathrm{s}} = \delta J_{\mathrm{s}}/(wH)$, and the response coefficient is obtained from $M_{\mathrm{de}} = \delta j_{\mathrm{s}}/E$. Finally, using Eq. (24), where $S = wH$ and $P = 2w$, one obtains the expression for the diffusio-osmotic conductivity:

$$K_{\mathrm{osm}} = \frac{k_{\mathrm{B}} T q_e}{4\pi \ell_{\mathrm{B}} \eta} \int_0^{\infty} \left\{ n_+(z) + n_-(z) - 2n_{\mathrm{s}} \frac{n_{\mathrm{w}}(z)}{n_{\mathrm{w}}^{\mathrm{b}}} \right\} \left[\phi(z) - \phi_{\mathrm{s}} - 2\,\mathrm{sgn}(\Sigma) \frac{b}{\ell_{\mathrm{GC}}} \right] \mathrm{d}z. \tag{30}$$

6 Modified Poisson-Boltzmann description

Following Refs. S29–S31, the mPB equation for a planar surface including ion-specific free energy profiles, $\Delta G_{\pm}(z)$, and a spatial dependence of the relative dielectric permittivity, $\varepsilon_r(z)$, is expressed as:

$$\varepsilon_0 \frac{\mathrm{d}}{\mathrm{d}z} \varepsilon_r(z) \frac{\mathrm{d}}{\mathrm{d}z} V(z) = -q_e \left[n_+(z) - n_-(z) \right] \tag{31}$$

$$= -q_e n_{\mathrm{s}} \left[e^{(-q_e V(z) - \Delta G_+(z))/k_B T} - e^{(q_e V(z) - \Delta G_-(z))/k_B T} \right]. \tag{32}$$

Assuming, as was done in the main text, that $\varepsilon_r(z)$ does not depend on the distance from the sheets and that is equal to the water dielectric constant, $\varepsilon_r = 78$, the mPB equation

reads:

$$\frac{\mathrm{d}^2\phi}{\mathrm{d}z^2} = -4\pi\ell_\mathrm{B}\left[n_+(z) - n_-(z)\right] = -4\pi\ell_\mathrm{B}n_\mathrm{s}\left[e^{-\phi(z)-g_+(z)} - e^{\phi(z)-g_-(z)}\right], \tag{33}$$

where we introduced the Bjerrum length $\ell_\mathrm{B} = q_e^2/(4\pi\varepsilon_0\varepsilon_r k_\mathrm{B}T)$ and dimensionless free energies of ion adsorption. The assumption of a constant dielectric permittivity at the aqueous interface is based on solid theoretical grounds which support the empirical evidence that the dielectric constant of a polar fluid is an intrinsic quantity.[S32,S33] Nevertheless, we have also tested the potential effect of a spatial dependence of the dielectric permittivity on the osmotic transport coefficients using a step-polarization model for $\varepsilon(z)$,[S19,S29] where $\varepsilon(r) = \varepsilon_0[(\varepsilon_r - 1)\theta(z - \tilde{z}) + 1]$, with $\theta(z - \tilde{z})$ being the Heaviside function centered at the height $\tilde{z}$. Here, $\tilde{z}$ is obtained from the conditions that the electric field in the vacuum-like region between the sheets and the first water density profile is zero when approached from the "left" side but it is non-zero when approached from the "right" side, that is:

$$\lim_{z\to\tilde{z}^-} \frac{\mathrm{d}\phi}{\mathrm{d}z} \to 0 \ \text{ and} \tag{34}$$

$$\lim_{z\to\tilde{z}^+} \frac{\mathrm{d}\phi}{\mathrm{d}z} \to \left.\frac{\mathrm{d}\phi}{\mathrm{d}z}\right|_{z=z^+}, \tag{35}$$

with $\left.\frac{\mathrm{d}\phi}{\mathrm{d}z}\right|_{z=z^+}$ being generally different from zero, thus implying a discontinuity in the electric field at $\tilde{z}$. The electrostatic potential is instead continuous at $\tilde{z}$ and equivalent to the surface potential ϕ_s – *i.e.* $\phi(z \to \tilde{z}^-) = \phi(z \to \tilde{z}^+) = \phi_\mathrm{s}$. In practice, in our simulations we have determined $\tilde{z}$ to be $\tilde{z} \approx 0.33$ nm for both the graphene and hBN aqueous interfaces. In Fig. S4, it can be seen that the ζ-potential and D_DO are not significantly affected by a possible distance dependence of the dielectric permittivity. A change is observed in the diffusio-osmotic conductivity K_{osm}, instead. Despite this change, a sign inversion in K_{osm} is observed for hBN at approximately 1 M regardless of the choice made for the dielectric permittivity.

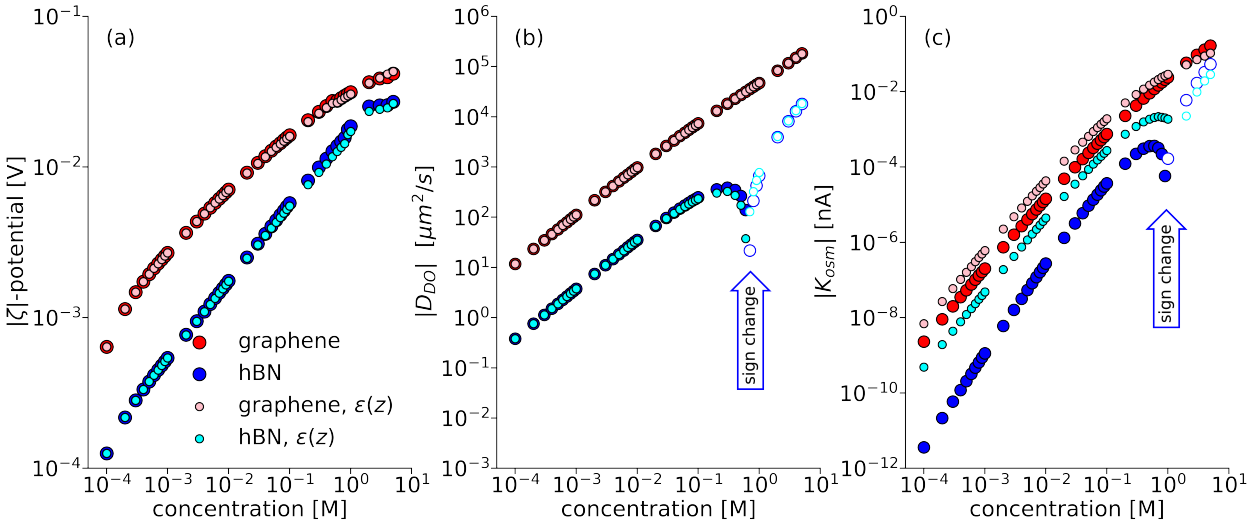

Figure S4: Scaling behaviour of the ζ-potential (a), diffusio-osmotic coefficient D_{DO} (b) and diffusio-osmotic conductivity K_{osm} (c) obtained with a constant value of the relative dielectric permittivity ($\varepsilon_r = 78$) as shown in the main text (red and blue symbols), and with a distance-dependent dielectric permittivity $\varepsilon(z)$ according to the step-polarization model (pink and cyan symbols). In (b) and (c) filled (empty) symbols refer to transport coefficients with a positive (negative) sign.

7 Effective surface charge model

In this section we will derive simplified expressions for the transport coefficients when the layer where ions and water interact specifically with the wall (adsorption layer) is very thin as compared to the characteristic lengths of the EDL; one can then integrate the ion-specific and water-specific contributions and use them as surface terms for a regular Poisson-Boltzmann description outside the adsorption layer.

7.1 Effective surface charge and surface potential

Within the mPB description, the charge density writes: $\rho_{\mathrm{e}}(z) = q_e n_{\mathrm{s}} \left[e^{-\phi(z)-g_+(z)} - e^{\phi(z)-g_-(z)}\right]$. One can rewrite the charge density as the sum of the standard PB expression and a correction due to specific interactions:

$$\rho_{\mathrm{e}} = q_e n_{\mathrm{s}} \left[e^{-\phi(z)} - e^{\phi(z)}\right] + q n_{\mathrm{s}} \left[e^{-\phi(z)} \left(e^{-g_+(z)} - 1\right) - e^{\phi(z)} \left(e^{-g_-(z)} - 1\right)\right], \qquad (36)$$

where $\left(e^{-g_+(z)}-1\right)$ and $\left(e^{-g_-(z)}-1\right)$ vanish outside the adsorption layer. Accordingly, the second term in Eq. (36) corresponds to a thin layer of specifically adsorbed ions, outside of which ions follow the standard PB equation. If the characteristic scale for the variation of the potential is much larger than the thickness of the adsorption layer, one can approximate the second term as a Dirac distribution of charge density located at the wall:

$$\rho_{\rm e} = q_e n_{\rm s}\left[e^{-\phi(z)} - e^{\phi(z)}\right] + \Sigma_{\rm eff}\delta(z), \text{ with} \tag{37}$$

$$\Sigma_{\rm eff} = \int_0^\infty q_e n_{\rm s}\left[e^{-\phi_{\rm s}}\left(e^{-g_+(z)}-1\right) - e^{\phi_{\rm s}}\left(e^{-g_-(z)}-1\right)\right]\,{\rm d}z \tag{38}$$

$$\Sigma_{\rm eff} = q_e n_{\rm s}\left[e^{-\phi_{\rm s}}K_+ - e^{\phi_{\rm s}}K_-\right], \tag{39}$$

where

$$K_+ = \int_0^\infty \left(e^{-g_+(z)}-1\right)\,{\rm d}z \quad \text{and} \quad K_- = \int_0^\infty \left(e^{-g_-(z)}-1\right)\,{\rm d}z \tag{40}$$

are characteristic length scales quantifying the amount of adsorbed ions.

Within the standard PB framework, one can then relate the surface potential to the effective surface charge through Grahame equation:[S28]

$$\sinh\left(\frac{\phi_{\rm s}}{2}\right) = 2\pi\ell_{\rm B}\lambda_{\rm D}\,\frac{\Sigma_{\rm eff}}{q} = \frac{1}{4\lambda_{\rm D}}\left[e^{-\phi_{\rm s}}K_+ - e^{\phi_{\rm s}}K_-\right]. \tag{41}$$

In the limit of small surface potential, $\phi_{\rm s} \ll 1$, one can linearize this equation, and compute $\phi_{\rm s}$:

$$\phi_{\rm s} \approx \frac{K_+ - K_-}{2\lambda_D + K_+ + K_-}. \tag{42}$$

7.2 Electro-osmosis

We start from the integral expression of the zeta potential, Eq. (4). Because the surface is electrically neutral, $\int_0^\infty b\rho_{\rm e}{\rm d}z = -b\Sigma = 0$, so that the slip length disappears from Eq. (4).

Using Eq. (36), ζ writes:

$$\zeta = -\frac{q n_\mathrm{s}}{\varepsilon}\left\{\int_0^\infty \left[e^{-\phi(z)} - e^{\phi(z)}\right] z\,\mathrm{d}z + \int_0^\infty \left[e^{-\phi(z)}\left(e^{-g_+(z)}-1\right) - e^{\phi(z)}\left(e^{-g_-(z)}-1\right)\right] z\,\mathrm{d}z\right\}. \tag{43}$$

When the adsorption layer is thin as compared to the scale of the electric field variations, one can simplify the second integral:

$$\int_0^\infty \left[e^{-\phi(z)}\left(e^{-g_+(z)}-1\right) - e^{\phi(z)}\left(e^{-g_-(z)}-1\right)\right] z\,\mathrm{d}z \approx e^{-\phi_\mathrm{s}} K_+ L_+ - e^{\phi_\mathrm{s}} K_- L_-, \tag{44}$$

where

$$L_+ = \frac{1}{K_+}\int_0^\infty \left(e^{-g_+(z)}-1\right) z\,\mathrm{d}z \quad \text{and} \quad L_- = \frac{1}{K_-}\int_0^\infty \left(e^{-g_-(z)}-1\right) z\,\mathrm{d}z. \tag{45}$$

L_+ and L_- quantify the thickness of the adsorbed layer of cations and anions. One can estimate an order of magnitude for the second integral as $\Sigma_\mathrm{eff}/(q_e n_\mathrm{s}) \times L$, with $L = \max(|L_+|, |L_-|)$. The first integral can be evaluated using the standard PB equation,[S28] and one obtains finally:

$$\zeta = \frac{k_\mathrm{B}T}{q_e}\phi_\mathrm{s} - \frac{q n_\mathrm{s}}{\varepsilon}\mathcal{O}\left(\frac{\Sigma_\mathrm{eff} L}{q n_\mathrm{s}}\right) = \frac{k_\mathrm{B}T}{q_e}\phi_\mathrm{s}\left\{1 - \mathcal{O}\left(\frac{L}{\lambda}\right)\right\}, \tag{46}$$

where $\lambda = -\phi_\mathrm{s}/\mathrm{d}_z\phi|_{z=0}$ is a characteristic scale for the variations of the electric potential.[S28] If $L \ll \lambda$, the zeta potential can be approximated as:

$$\zeta \approx \frac{k_\mathrm{B}T}{q_e}\phi_\mathrm{s}, \tag{47}$$

with ϕ_s given by Eq. (42).

7.3 Diffusio-osmosis

We start from the integral expression of the diffusio-osmotic mobility, Eq. (11), which we rewrite as the sum of the standard PB expression and a contribution due to specific interac-

tions, *i.e.* $D_{\mathrm{DO}} = D_{\mathrm{DO}}^{\mathrm{PB}} + D_{\mathrm{DO}}^{\mathrm{ads}}$ where

$$\frac{D_{\mathrm{DO}}^{\mathrm{PB}}}{k_{\mathrm{B}}T} = \frac{n_{\mathrm{s}}}{\eta}\int_0^\infty \left[e^{-\phi(z)} + e^{\phi(z)} - 2\right](z+b)\,\mathrm{d}z, \tag{48}$$

$$\frac{D_{\mathrm{DO}}^{\mathrm{ads}}}{k_{\mathrm{B}}T} = \frac{n_{\mathrm{s}}}{\eta}\int_0^\infty \left[e^{-\phi(z)}\left(e^{-g_+(z)}-1\right) + e^{\phi(z)}\left(e^{-g_-(z)}-1\right) - 2\left(\frac{n_{\mathrm{w}}(z)}{n_{\mathrm{w}}^{\mathrm{b}}}-1\right)\right](z+b)\,\mathrm{d}z. \tag{49}$$

In the thin adsorption layer limit, $D_{\mathrm{DO}}^{\mathrm{PB}}$ can be computed using the standard PB equation,[S28,S34] while $D_{\mathrm{DO}}^{\mathrm{ads}}$ can be approximated in terms of characteristic adsorption lengths, to yield the expression presented in the main text:

$$\frac{D_{\mathrm{DO}}}{k_{\mathrm{B}}T} \approx \frac{1}{2\pi\ell_{\mathrm{B}}\eta}\left\{-\ln\left(1-\gamma^2\right) + \frac{b|\gamma|}{\ell_{\mathrm{GC}}^{\mathrm{eff}}} + \frac{1}{4\lambda_{\mathrm{D}}^2}\left[e^{-\phi_{\mathrm{s}}}K_+L_+ + e^{\phi_{\mathrm{s}}}K_-L_- - 2K_{\mathrm{w}}L_{\mathrm{w}} + b\left(e^{-\phi_{\mathrm{s}}}K_+ + e^{\phi_{\mathrm{s}}}K_- - 2K_{\mathrm{w}}\right)\right]\right\}, \tag{50}$$

where $\gamma = \tanh\left(\phi_{\mathrm{s}}/4\right)$, and $\ell_{\mathrm{GC}}^{\mathrm{eff}} = q_e/(2\pi\ell_{\mathrm{B}}|\Sigma_{\mathrm{eff}}|)$ is the effective Gouy-Chapman length corresponding to the effective surface charge.

7.3.1 Scaling of the Diffusio-osmotic coefficient

The diffusio-osmotic coefficient D_{DO} scales approximately linearly with n_{s} on graphene at all concentrations considered, whereas on hBN deviations from linearity appear above 10^{-1} M, and a sign reversal is seen at concentrations just below 1 M. We present the concentration dependence of the diffusio-osmotic coefficient and the contributions coming from $D_{\mathrm{DO}}^{\mathrm{PB}}$ and from $D_{\mathrm{DO}}^{\mathrm{ads}}$ in Fig. S5. The main PB contribution to D_{DO} is determined by the slippage term in Eq. (50), which on hBN scales as $D_{\mathrm{DO}}^{\mathrm{PB}} \propto n_{\mathrm{s}}^{3/2}$, given that $\gamma \propto \phi_{\mathrm{s}}$ and that the surface potential scales with the square root of the concentration ($\phi_{\mathrm{s}} \propto \sqrt{n_{\mathrm{s}}}$), while on graphene, $D_{\mathrm{DO}}^{\mathrm{PB}}$ scales with a slightly smaller exponent than $n_{\mathrm{s}}^{3/2}$ because ϕ_{s} also scales more slowly than $\sqrt{n_{\mathrm{s}}}$ (see also the main text). As reported in the main text, at low concentrations the specific adsorption contribution $D_{\mathrm{DO}}^{\mathrm{ads}}$ scales linearly with salt concentration and is also determined

by the term proportional to the slip-length in Eq. (50) given by $b\left(e^{-\phi_s}K_+ + e^{\phi_s}K_- - 2K_w\right)$. At concentrations of about 1 M, competing effects between the water-specific and the ion-specific interactions lead to a sign change in D_{DO}^{ads} for both graphene and hBN (see symbols in Fig. S3(c)). The sign reversal of D_{DO}^{ads} is offset by the amplifying slip effect arising from the PB term proportional to $b|\gamma|/l_{GC}^{eff}$, but while on graphene this term is sufficiently large such that D_{DO} is positive at all concentrations considered, this is not the case for hBN such that a sign reversal is observed on hBN at concentrations of just below 1 M (see Fig. S3(a)).

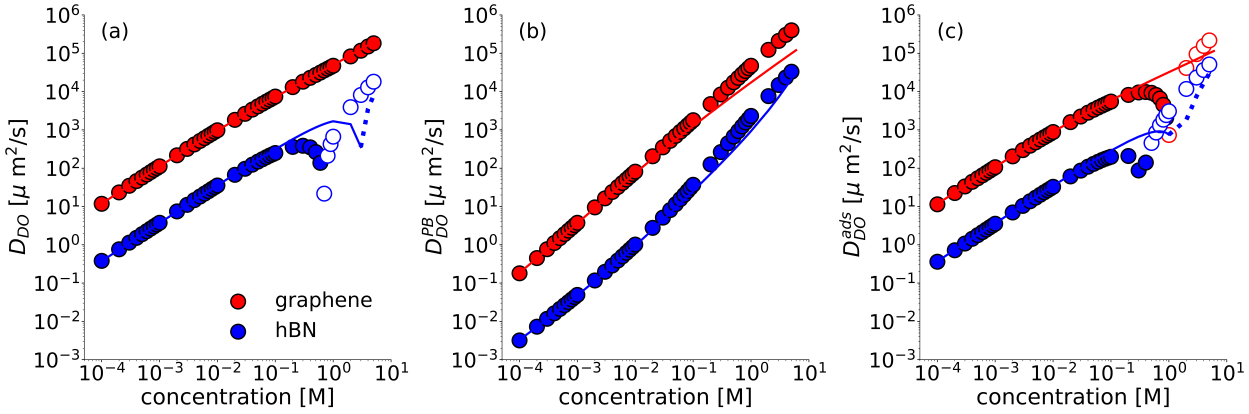

Figure S5: Concentration dependence of the diffusio-osmotic coefficient for the aqueous graphene and aqueous hBN interfaces as shown in the main text (a), alongside the contributions coming from D_{DO}^{PB} (b) and from D_{DO}^{ads} (c). Filled (empty) symbols and solid (dotted) lines refer to positive (negative) values of the response coefficients.

7.4 Diffusio-osmotic current

We start from the expression of K_{osm} in Eq. (30), which we simplify by noting that the slip contribution vanishes for a neutral surface:

$$K_{osm} = \frac{k_B T q_e n_s}{4\pi \ell_B \eta}\left\{\int_0^\infty \left[e^{-\phi(z)} + e^{\phi(z)} - 2\right](\phi(z) - \phi_s)\,dz + \right.$$
$$\left.\int_0^\infty \left[e^{-\phi(z)}\left(e^{-g_+(z)} - 1\right) + e^{\phi(z)}\left(e^{-g_-(z)} - 1\right) - 2\left(\frac{n_w(z)}{n_w^b} - 1\right)\right](\phi(z) - \phi_s)\,dz\right\} \quad (51)$$

In the thin adsorption layer limit, the first integral, which we denote $K_{\mathrm{osm}}^{\mathrm{PB}}$, can be computed using the standard PB equation:[S28,S34]

$$K_{\mathrm{osm}}^{\mathrm{PB}} = \frac{k_{\mathrm{B}}Tq_e n_{\mathrm{s}}}{4\pi\ell_{\mathrm{B}}\eta}\int_0^\infty \left[e^{-\phi(z)}+e^{\phi(z)}-2\right](\phi(z)-\phi_{\mathrm{s}})\,\mathrm{d}z \approx \frac{k_{\mathrm{B}}Tq_e}{4\pi\ell_{\mathrm{B}}\eta}\frac{1}{8\pi\ell_{\mathrm{B}}}\int_0^\infty \left(\frac{\mathrm{d}\phi}{\mathrm{d}z}\right)^2(\phi(z)-\phi_{\mathrm{s}})\,\mathrm{d}z = -\frac{k_{\mathrm{B}}T\Sigma_{\mathrm{eff}}}{2\pi\ell_{\mathrm{B}}\eta}\left(1-\frac{\operatorname{asinh}\chi}{\chi}\right). \quad (52)$$

To express second integral in Eq. (51) in terms of the characteristic adsorption lengths, we further assume that the difference $\phi(z)-\phi_{\mathrm{s}}$ can be linearized for z close to $\tilde{z}$, where $\tilde{z}$ has been defined in Eqs. (34) and (35). This approximation reads:

$$\phi(z)-\phi_{\mathrm{s}} \approx 0 \quad \text{for } z<\tilde{z} \text{ and} \quad (53)$$

$$\phi(z)-\phi_{\mathrm{s}} \approx \left.\frac{\mathrm{d}\phi}{\mathrm{d}z}\right|_{z=\tilde{z}^+}(z-\tilde{z}) = -\frac{2\,\mathrm{sgn}\,(\Sigma_{\mathrm{eff}})}{\ell_{\mathrm{GC}}}(z-\tilde{z}) \quad \text{for } z\geq\tilde{z}. \quad (54)$$

The above conditions allow us to introduce a new set of characteristic lengths analogous to those defined in Table 1 in the main text:

$$\tilde{K}_+ = \int_{\tilde{z}}^\infty \left(e^{-g_+(z)}-1\right)\mathrm{d}z \qquad \tilde{K}_- = \int_{\tilde{z}}^\infty \left(e^{-g_-(z)}-1\right)\mathrm{d}z \quad (55)$$

$$\tilde{L}_+ = \frac{1}{\tilde{K}_+}\int_{\tilde{z}}^\infty \left(e^{-g_+(z)}-1\right)(z-\tilde{z})\,\mathrm{d}z \qquad \tilde{L}_- = \frac{1}{\tilde{K}_-}\int_{\tilde{z}}^\infty \left(e^{-g_-(z)}-1\right)(z-\tilde{z})\,\mathrm{d}z \quad (56)$$

$$\tilde{K}_w = \int_{\tilde{z}}^\infty \left(\frac{n_{\mathrm{w}}(z)}{n_{\mathrm{w}}^{\mathrm{b}}}-1\right)\mathrm{d}z \qquad \tilde{L}_w = \frac{1}{\tilde{K}_w}\int_{\tilde{z}}^\infty \left(\frac{n_{\mathrm{w}}(z)}{n_{\mathrm{w}}^{\mathrm{b}}}-1\right)(z-\tilde{z})\,\mathrm{d}z. \quad (57)$$

We then denote the second integral in Eq. (51) as $K_{\mathrm{osm}}^{\mathrm{ads}}$ and express it in terms of these characteristic lengths as:

$$K_{\mathrm{osm}}^{\mathrm{ads}} = \frac{k_{\mathrm{B}}Tq_e n_{\mathrm{s}}}{4\pi\ell_{\mathrm{B}}\eta}\int_0^\infty \left[e^{-\phi(z)}\left(e^{-g_+(z)}-1\right)+e^{\phi(z)}\left(e^{-g_-(z)}-1\right)-2\left(\frac{n_{\mathrm{w}}(z)}{n_{\mathrm{w}}^{\mathrm{b}}}-1\right)\right] \times(\phi(z)-\phi_{\mathrm{s}})\,\mathrm{d}z \approx -\frac{k_{\mathrm{B}}T\Sigma_{\mathrm{eff}}}{2\pi\ell_{\mathrm{B}}\eta}\cdot\frac{e^{-\phi_{\mathrm{s}}}\tilde{K}_+\tilde{L}_+ + e^{\phi_{\mathrm{s}}}\tilde{K}_-\tilde{L}_- - 2\tilde{K}_{\mathrm{w}}\tilde{L}_{\mathrm{w}}}{4\lambda_D^2}. \quad (58)$$

Substituting Eq. (58) and (52) to Eq. (51) we obtain the final expression of the ESC model for $K_{\rm osm}$ reported in the main text:

$$K_{\rm osm} \approx -\frac{k_{\rm B}T\Sigma_{\rm eff}}{2\pi\ell_{\rm B}\eta} \times \left(1 - \frac{\sinh^{-1}\chi}{\chi} + \frac{e^{-\phi_{\rm s}}\tilde{K}_{+}\tilde{L}_{+} + e^{\phi_{\rm s}}\tilde{K}_{-}\tilde{L}_{-} - 2\tilde{K}_{\rm w}\tilde{L}_{\rm w}}{4\lambda_D^2}\right). \tag{59}$$

7.4.1 Scaling of Diffusio-osmotic conductivity

As discussed in the main text, the diffusio-osmotic conductivity at concentrations between 10^{-4} and 10^{-1} M scales as $K_{\rm osm} \sim n_{\rm s}^{p}$, with $p \approx 2$ and $p \approx 2.5$ for graphene and hBN, respectively. To illustrate the origin of the different scaling behaviour in the two materials, we present the concentration dependence of the diffusio-osmotic conductivity and the contributions coming from $K_{\rm osm}^{\rm PB}$ and from $K_{\rm osm}^{\rm ads}$ (see definitions in previous section) in Fig. S6. On graphene, both $K_{\rm osm}^{\rm PB}$ and $K_{\rm osm}^{\rm ads}$ scale approximately quadratically for $n_{\rm s} \in [10^{-4}; 10^{-1}]$ M. On hBN $K_{\rm osm}^{\rm PB}$ also scales quadratically with salt concentration, whereas the scaling of $K_{\rm osm}^{\rm ads}$ is more complex at low concentrations, where a sign change from negative to positive is observed at about 5×10^{-3} M. Accordingly, at very low salt concentration $K_{\rm osm}^{\rm ads}$ goes against $K_{\rm osm}^{\rm PB}$, while above 5×10^{-3} M $K_{\rm osm}^{\rm ads}$ goes with $K_{\rm osm}^{\rm PB}$; this results in an effective scaling law for the total response with a power larger than the standard $p = 2$ value.

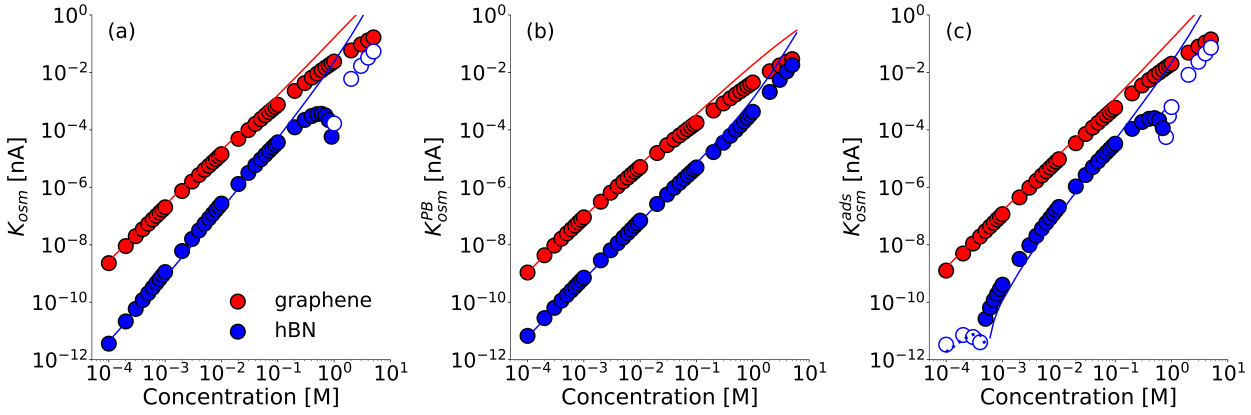

Figure S6: Concentration dependence of the diffusio-osmotic conductivity for the aqueous graphene and aqueous hBN interfaces as shown in the main text (a), alongside the contributions coming from $K_{\rm osm}^{\rm PB}$ (b) and from $K_{\rm osm}^{\rm ads}$ (c). Filled (empty) symbols and solid (dotted) lines refer to positive (negative) values of the response coefficients.

8 Summary of characteristic lengths

The characteristic lengths of the ESC model are reported in Table S3.

Table S3: Slip lengths (b) and length-scales characteristic of cation-specific (with subscripts "+"), anion-specific adsorption (with subscripts "−") and water density oscillations (with subscript "w") at the aqueous graphene and hBN interfaces, along with their definitions. The lengths with the " ˜ " are relevant to the calculation of the diffusio-osmotic conductivity – where $\tilde{z} = 0.33$ nm – and are only reported here for ease of presentation, whereas the other lengths are also shown in the main text. The slip-length and the anion length-scales are in bold to highlight the stark differences between graphene and hBN.

lengths [nm]	definition	graphene	hBN
$\boldsymbol{b}$		**+19.6**	**+4.0**
K_+	$\int_0^\infty [e^{-g_+(z)} - 1]\mathrm{d}z$	−0.229	−0.207
$\boldsymbol{K_-}$	$\int_0^\infty [e^{-g_-(z)} - 1]\mathrm{d}z$	**+1.974**	**+0.177**
K_w	$\int_0^\infty [n_w(z)/n_w^b - 1]\mathrm{d}z$	−0.179	−0.165
L_+	$K_+^{-1} \int_0^\infty z[e^{-g_+(z)} - 1]\mathrm{d}z$	−0.363	−0.442
$\boldsymbol{L_-}$	$K_-^{-1} \int_0^\infty z[e^{-g_-(z)} - 1]\mathrm{d}z$	**+0.459**	**−0.099**
L_w	$K_w^{-1} \int_0^\infty z[n_w(z)/n_w^b - 1]\mathrm{d}z$	−0.031	−0.027
$\tilde{K}_+$	$\int_{\tilde{z}}^\infty [e^{-g_+(z)} - 1]\mathrm{d}z$	+0.085	+0.106
$\boldsymbol{\tilde{K}_-}$	$\int_{\tilde{z}}^\infty [e^{-g_-(z)} - 1]\mathrm{d}z$	**+2.067**	**+0.375**
$\tilde{K}_w$	$\int_{\tilde{z}}^\infty [n_w(z)/n_w^b - 1]\mathrm{d}z$	+0.012	+0.019
$\tilde{L}_+$	$\tilde{K}_+^{-1} \int_{\tilde{z}}^\infty (z - \tilde{z})[e^{-g_+(z)} - 1]\mathrm{d}z$	+1.227	+0.989
$\boldsymbol{\tilde{L}_-}$	$\tilde{K}_-^{-1} \int_{\tilde{z}}^\infty (z - \tilde{z})[e^{-g_-(z)} - 1]\mathrm{d}z$	**+0.099**	**−0.248**
$\tilde{L}_w$	$\tilde{K}_w^{-1} \int_{\tilde{z}}^\infty (z - \tilde{z})[n_w(z)/n_w^b - 1]\mathrm{d}z$	+0.222	+0.424

References

(S1) Hutter, J.; Iannuzzi, M.; Schiffmann, F.; VandeVondele, J. CP2K: Atomistic Simulations of Condensed Matter Systems. *Wiley Inter Rev: Comp Mol Sci* **2013**, *4*, 15–25.

(S2) Kühne, T. D.; Iannuzzi, M.; Del Ben, M.; Rybkin, V. V.; Seewald, P.; Stein, F.; Laino, T.; Khaliullin, R. Z.; Schütt, O.; Schiffmann, F.; Golze, D.; Wilhelm, J.; Chulkov, S.; Bani-Hashemian, M. H.; Weber, V.; Borštnik, U.; Taillefumier, M.; Jakobovitz, A. S.; Lazzaro, A.; Pabst, H.; *et al.*, CP2K: An Electronic Structure and Molecular Dynamics Software Package-Quickstep: Efficient and Accurate Electronic Structure Calculations. *The Journal of Chemical Physics* **2020**, *152*, 194103.

(S3) Lippert, G.; Hutter, J.; Parrinello, M. A Hybrid Gaussian and Plane Wave Density Functional Scheme. *Mol. Phys.* **1997**, *92*, 477.

(S4) Goedecker, S.; Teter, M.; Hutter, J. Separable Dual-Space Gaussian Pseudopotentials. *Phys. Rev. B* **1996**, *54*, 1703–1710.

(S5) VandeVondele, J.; Hutter, J. Gaussian Basis Sets for Accurate Calculations on Molecular Systems in Gas and Condensed Phases. *J. Chem. Phys.* **2007**, *127*, 114105.

(S6) Lide, D. R. *CRC Handbook of Chemistry and Physics*; CRC press: Boca Raton, Florida, 2004.

(S7) Paszkowicz, W.; Pelka, J.; Knapp, M.; Szyszko, T.; Podsiadlo, S. Lattice Parameters and Anisotropic Thermal Expansion of Hexagonal Boron Nitride in the 10–297.5 K Temperature Range. *Appl. Phys. A* **2002**, *75*, 431–435.

(S8) Torrie, G. M.; Valleau, J. P. Nonphysical Sampling Distributions in Monte Carlo Free-energy Estimation: Umbrella Sampling. *Journal of Computational Physics* **1977**, *23*, 187–199.

(S9) Martyna, G.; Klein, M. L.; Tuckerman, M. E. Nosé-Hoover Chains: The Canonical Ensemble *via* Continuous Dynamics. *J. Chem. Phys.* **1992**, *97*, 2635.

(S10) Kästner, J. Umbrella Sampling. *Wiley Interdisciplinary Reviews: Computational Molecular Science* **2011**, *1*, 932–942.

(S11) Tocci, G.; Bilichenko, M.; Joly, L.; Iannuzzi, M. *Ab Initio* Nanofluidics: Disentangling the Role of the Energy Landscape and of Density Correlations on Liquid/Solid Friction. *Nanoscale* **2020**, *12*, 10994–11000.

(S12) Berendsen, H. J. C.; Grigera, J. R.; Straatsma, T. P. The Missing Term in Effective Pair Potentials. *J. Phys. Chem.* **1987**, *91*, 6269.

(S13) Mayo, S. L.; Olafson, B. D.; Goddard III, W. A. DREIDING: A Generic Force Field for Molecular Simulations. *J. Phys. Chem.* **1990**, *94*, 8897.

(S14) Rajan, A. G.; Strano, M. S.; Blankschtein, D. *Ab Initio* Molecular Dynamics and Lattice Dynamics-Based Force Field for Modelling Hexagonal Boron Nitride in Mechanical and Interfacial Applications. *J. Chem. Phys.* **2018**, *9*, 1584–1591.

(S15) Werder, T.; Walther, J. H.; Jaffe, R. L.; Halicioglu, T.; Koumoutsakos, P. On the Water-Carbon Interaction for Use in Molecular Dynamics Simulations of Graphite and Carbon Nanotubes. *J. Phys. Chem. B* **2003**, *107*, 1345.

(S16) McCaffrey, D. L.; Nguyen, S. C.; Cox, S. J.; Weller, H.; Alivisatos, A. P.; Geissler, P. L.; Saykally, R. J. Mechanism of Ion Adsorption to Aqueous Interfaces: Graphene/Water *vs.* Air/Water. *Proceedings of the National Academy of Sciences* **2017**, *114*, 13369–13373.

(S17) Joung, I. S.; Cheatham III, T. E. Determination of Alkali and Halide Monovalent Ion Parameters for Use in Explicitly Solvated Biomolecular Simulations. *The Journal of Physical Chemistry B* **2008**, *112*, 9020–9041.

(S18) Le, J.; Iannuzzi, M.; Cuesta, A.; Cheng, J. Determining Potentials of Zero Charge of Metal Electrodes *versus* the Standard Hydrogen Electrode from Density-Functional-Theory-Based Molecular Dynamics. *Physical Review Letters* **2017**, *119*, 016801.

(S19) Huang, D. M.; Cottin-Bizonne, C.; Ybert, C.; Bocquet, L. Ion-Specific Anomalous Electrokinetic Effects in Hydrophobic Nanochannels. *Physical Review Letters* **2007**, *98*, 177801.

(S20) Marbach, S.; Bocquet, L. Osmosis, from Molecular Insights to Large-Scale Applications. *Chemical Society Reviews* **2019**, *48*, 3102–3144.

(S21) Bonthuis, D. J.; Netz, R. R. Beyond the Continuum: How Molecular Solvent Structure Affects Electrostatics and Hydrodynamics at Solid–Electrolyte Interfaces. *The Journal of Physical Chemistry B* **2013**, *117*, 11397–11413.

(S22) Bocquet, L.; Barrat, J.-L. Flow Boundary Conditions from Nano- to Micro-Scales. *Soft Matter* **2007**, *3*, 685–693.

(S23) Liu, Y.; Ganti, R.; Frenkel, D. Pressure Gradients Fail to Predict Diffusio-Osmosis. *Journal of Physics: Condensed Matter* **2018**, *30*, 205002.

(S24) Onsager, L. Reciprocal Relations in Irreversible Processes. I. *Physical Review* **1931**, *37*, 405–426.

(S25) Onsager, L. Reciprocal Relations in Irreversible Processes. II. *Physical Review* **1931**, *38*, 2265–2279.

(S26) Anderson, J. Colloid Transport By Interfacial Forces. *Annual Review of Fluid Mechanics* **1989**, *21*, 61–99.

(S27) Lee, C.; Cottin-Bizonne, C.; Biance, A.-L.; Joseph, P.; Bocquet, L.; Ybert, C. Osmotic Flow through Fully Permeable Nanochannels. *Physical Review Letters* **2014**, *112*, 244501.

(S28) Herrero, C.; Joly, L. Poisson-Boltzmann Formulary. 2021, 2105.00720, arXiv. `https://arxiv.org/abs/2105.00720`, (accessed May 3, 2021).

(S29) Schwierz, N.; Horinek, D.; Netz, R. R. Reversed Anionic Hofmeister Series: The Interplay of Surface Charge and Surface Polarity. *Langmuir* **2010**, *26*, 7370–7379.

(S30) Luo, G.; Malkova, S.; Yoon, J.; Schultz, D. G.; Lin, B.; Meron, M.; Benjamin, I.; Vanỳsek, P.; Schlossman, M. L. Ion Distributions near a Liquid-Liquid Interface. *Science* **2006**, *311*, 216–218.

(S31) Boström, M.; Tavares, F. W.; Finet, S.; Skouri-Panet, F.; Tardieu, A.; Ninham, B. Why Forces between Proteins Follow Different Hofmeister Series for PH above and Below PI. *Biophysical Chemistry* **2005**, *117*, 217–224.

(S32) Chandler, D. The Dielectric Constant and Related Equilibrium Properties of Molecular Fluids: Interaction Site Cluster Theory Analysis. *The Journal of Chemical Physics* **1977**, *67*, 1113–1124.

(S33) Cox, S. J. Dielectric Response with Short-Ranged Electrostatics. *Proceedings of the National Academy of Sciences* **2020**, *117*, 19746–19752.

(S34) Mouterde, T.; Bocquet, L. Interfacial Transport with Mobile Surface Charges and Consequences for Ionic Transport in Carbon Nanotubes. *The European Physical Journal E* **2018**, *41*, 148.